Numerical Analysis of Chaos in a Phononic Crystal Waveguide with Circular Inclusions of Real Materials

A. Bucio-Gutiérrez [ID] [α,1], **H. Pérez-Aguilar** [ID] [α,2] **and H. E. Alva-Medrano** [ID] [β,3]

[α]Facultad de Ciencias Físico Matemáticas, UMSNH, Av. Francisco J. Múgica S/N, 58030, Morelia, Michoacán, México, [β]Tecnológico Nacional de México, Instituto Tecnológico de Morelia, Avenida Tecnológico 1500, 58120, Morelia, Michoacán, México.

ABSTRACT Phononic crystal waveguides (PnCW) have been of great interest due to their properties of manipulating or filtering the acoustic waves with which they interact. Similarly, the presence of the phenomenon of chaos in the classical transport of particles through billiards with analogous geometries has been investigated. With this in consideration, in the present work an acoustic system of a two-dimensional PnCW is modeled, composed of two plane-parallel plates and a periodic arrangement of circular cylindrical inclusions with acoustic surfaces of real materials. In this system, we use the numerical technique of the integral equation, which allows us to obtain the pressure field corresponding to the normal modes in a range of frequencies. In addition, spatial statistical properties of pressure intensity such as the autocorrelation function (ACF) and its standard deviation called correlation length were calculated. The results show that when the correlation length is very small, the system presents disordered patterns of field intensities. Thus under certain conditions, the system under consideration presents a chaotic behavior, similar to the corresponding classical system.

INTRODUCTION

A phononic crystal (PnC) is a periodic material that exhibits a forbidden band structure for certain frequency ranges of acoustic waves (Maldovan 2013). This feature allows effective control of sound propagation, as waves cannot propagate in certain directions or specific frequency ranges. These bands are determined by the geometric parameters and the elastic properties of the material used in the PnC (Khelif et al. 2004). The constant study of the properties of PnCs has allowed the development of structures that offer optimal control over wave propagation. Thanks to this, advanced devices such as acoustic diodes, waveguides (Otsuka et al. 2013), selective filters, and acoustic superlenses (Chen et al. 2018) have been manufactured, among others.

Among these devices, waveguides stand out as they are used in various scientific and technological fields; such as optics, in photonic circuits of nanometric order (Lee et al. 2016); and concerning this work, in acoustics, in phononic crystal waveguides (PnCWs).

PnCWs are systems composed of a periodic structure formed by two or more fluids, or a combination of solid and fluid, that interact with a pressure field. In fact, the crystalline structures that make up the PnCWs are fundamental in solid state physics (Kittel et al. 1996). That is why PnCW systems have emerged as a fascinating area of research in recent years. As these band structures exhibit properties such as the manipulation of acoustic wave propagation, which has shown great potential for the control and direction of acoustic waves in a wide range of applications.

The design of PnCW involves the manipulation of parameters such as geometry, spacing, and material composition (Jia et al. 2018). This allows the creation of specific frequency bands where acoustic waves can be confined and guided along predetermined paths. This ability to control sound propagation opens up a wide range of potential applications, ranging from acoustic signal processing devices (El-Kady et al. 2008) to noise isolation systems (Torrent and Sánchez-Dehesa 2008).

Similarly, there have been notable advances in the theoretical understanding, simulation, and manufacturing of PnCWs. Exhaustive research has been carried out on multiple waveguide configurations, ranging from one- to two-dimensional and three-dimensional (Pennec et al. 2010b; Liu et al. 2020). The literature has studied the response of PnC and PnCW systems made of different materials such as quartz whose acoustic response is in the order of

kiloHertz (He *et al.* 2020), lead-epoxy unit cell to detect different gases at different temperatures (Zaki *et al.* 2020), gas and water pipelines over the 1-50 kHz (Jing *et al.* 2018), stainless steel with mechanically drilled holes filled with liquid for its characterization by measuring its bulk modulus (Mukhin *et al.* 2022). These advances have allowed a greater understanding of the fundamental principles that govern the behavior of waves in these systems, as well as the development of more sophisticated techniques for their design and manufacture.

Additionally, it is important to note that PnCs share various similarities with photonic crystals (PC). One of these similarities is the simultaneous existence of forbidden bands for both photons and phonons (Pennec *et al.* 2010a). This connection between PnCs and PCs has led us to the hypothesis that the former can also exhibit chaotic dynamics in systems of geometries similar to the latter (Navarro-Urrios *et al.* 2017). These observations open the door to new research and explorations in the field of phononic crystals, in search of better understanding of their behavior and take advantage of their properties for various purposes.

Classical fields (electromagnetic, acoustic, etc.) or quantum amplitude probabilities share the same interesting statistical features when, in the corresponding geometrical or classical limits (wavelength tends to zero), the dynamics of rays or trajectories exhibit chaos (Stöckmann 1999). Wave and quantum chaos are thus now well-documented topics covering a wide variety of physical systems: electrons in quantum dots (Wilkinson *et al.* 1996), cold atoms (Hensinger *et al.* 2001), surface waves (Kudrolli *et al.* 2001), elastodynamics (Weaver 1989), acoustics (de Rosny *et al.* 2000; Ellegaard *et al.* 2001), microwaves (Sridhar 1991; Dembowski *et al.* 2000) and optical cavities (Nöckel and Stone 1997; Doya *et al.* 2002a). In wave cavities for which the limit of rays exhibits chaos, wave function statistics is generally expected to follow the predictions of Random Matrix Theory (RMT). According to this theory, wave functions are uniformly distributed over the whole available phase space which is ergodically explored by the rays, thus locally resulting in a random superposition of plane waves (Berry 1977). Nevertheless, some ergodic modes of chaotic billiard systems are known to show an anomalous increase in intensity along weakly unstable periodic orbits, a phenomenon called scarring (Heller 1984; Kaplan 1998; Ellegaard *et al.* 2001; Doya *et al.* 2002a). Two alternative approaches are generally considered to study the influence of scars on wave statistics in chaotic wave cavities. One is devoted to the analysis of individual scarred eigenstates (Heller 1984), while the other is dynamical as it is based on the evolution of wave packets launched along periodic orbits (Kaplan and Heller 1999), that generally the long time evolution yields a typical specklelike field pattern characterized by the well-known isotropic field autocorrelation function (ACF) (Berry 1977; Doya *et al.* 2002a; Kuhl *et al.* 2005). In this context, it is relevant to highlight that the analysis of the ACF has proven to be a very useful tool for understanding and characterizing both theoretically and experimentally chaotic behavior. This technique has been particularly applied in the study of optical fibers with non-circular cross-sections, where light rays exhibit chaotic dynamics (Doya *et al.* 2002b).

There are advances in the theory of chaotic dynamical systems, particularly the results of Sinai (Sinai 1970) and Ruelle (Ruelle 1991), on wave mechanics experiments that use microwaves for studying the so-called quantum-classical correspondence, a central issue in quantum chaos. The properties of closed Sinai billiard microwave cavities have been discussed in terms of universal predictions from RMT, as well as periodic orbit contributions, which manifest as scars in eigenfunctions and standing wave patterns (Sridhar and Lu 2002). In an equivalent analogy we study the acoustic-classical correspondence of the properties of the eigenvalues and eigenfunctions of the Sinai billiard-shaped cavities and the 2-D n-disk billiards in PnCWs. Consequently, through the ACF, it is possible to obtain precise information about the statistical properties of the acoustic response of the study system. The ACF allows evaluating the similarity of a signal with itself as it moves both in time and space, especially in cases where the stationary case is assumed. In this way, the analysis of the ACF is positioned as a valuable tool to deepen the study of chaotic systems and contribute to a greater understanding of their dynamic behavior.

In our study, we have considered two acoustic systems of two-dimensional PnCWs, one of infinite length and another of truncated length. These systems are composed of two plane-parallel plates and a periodic arrangement of circular cylindrical inclusions with acoustic surfaces of particular materials, as illustrated in Figures 1 and 2. The inclusions play a crucial role in wave behavior, acting as reflectors and diffractors. This leads to a significant modification in the pressure field compared to the case of a PnCW having two plates with acoustic surfaces but no inclusions.

In our numerical simulations, we have used the Integral Equation Method (IEM) (Mendoza-Suárez and Pérez-Aguilar 2016; Villa-Villa *et al.* 2017), which has proven to be a powerful tool for analyzing acoustic response. This method has the advantage of considering interaction between two plane-parallel plates and cylindrical inclusions, allowing more accurate results. Through this technique, we can investigate and understand normal mode behavior in different geometric configurations and frequencies, specifically in our particular systems. This gives us greater ability to analyze the acoustic response of our system and allows us to obtain valuable information about its statistical properties.

METHODOLOGY

Firstly, it is necessary to find the equation that characterizes the problem posed. The wave equation is the central element that determines and conditions the propagation of acoustic waves in a given medium. For this, we consider the continuum theory in a homogeneous medium, which means that its properties in the unperturbed state are the same everywhere. We also consider the case of perfect fluids, as these do not deform nor allow the propagation of transverse mechanical waves, so processes such as energy dissipation due to viscosity are ignored. Therefore, a linear approximation is performed on the continuity equation of mass, the non-viscous force equation and the equation of state around an initial stationary state of the system (Blackstock 2001), obtaining

$$\frac{\partial s}{\partial t} + \nabla \cdot \mathbf{u} = 0, \tag{1a}$$

$$-\nabla p(\mathbf{r}, t) = \rho_0 \frac{\partial \mathbf{u}}{\partial t}, \tag{1b}$$

$$p = Bs, \tag{1c}$$

where $\mathbf{u}$ is the average vectorial velocity of the fluid, B is called the adiabatic volumetric modulus, s is the condensation at any point and p is the acoustic pressure at any point, considered harmonic in time. As acoustics studies the generation and spatio-temporal evolution of small mechanical perturbations (vibrations) in a fluid (sound waves) or in a solid (elastic waves), it is natural to describe the behavior of the acoustic pressure field in the waveguide through the Helmholtz equation, similar to Maxwell equations in electromagnetic system, from Eqs. (1). Thus, applying the diver-
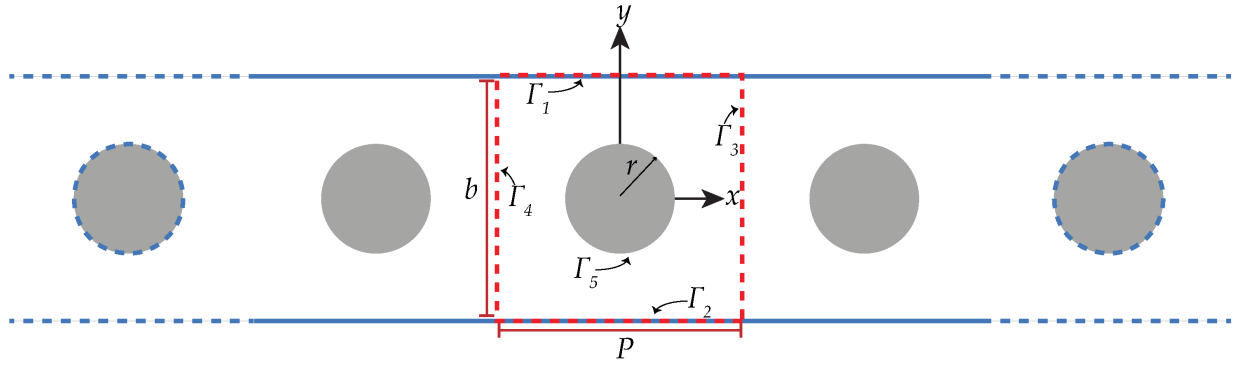
Figure 1 Infinite 2D PnCW system diagram. The system is composed of two plane-parallel plates and a periodic arrangement of circular cylindrical inclusions with acoustic surfaces. The Γ contours define the unit cell of the system with periodicity in the x-direction.

gence to Eq. (1a), we obtain

$$-\nabla^2 p(\mathbf{r}, t) = \rho_0 \nabla \cdot \frac{\partial \mathbf{u}}{\partial t}, \tag{2}$$

where ∇^2 is the three-dimensional Laplacian operator. On the other hand, considering the temporal derivative of Eq. (1a) and using $\partial(\nabla \cdot \mathbf{u})/\partial t = \nabla \cdot (\partial \mathbf{u}/\partial t)$, we arrive at

$$\frac{\partial^2 s}{\partial t^2} + \nabla \cdot \frac{\partial \mathbf{u}}{\partial t} = 0. \tag{3}$$

Now, combining Eqs. (2) and (3), can be reduced to

$$\nabla^2 p(\mathbf{r}, t) = \rho_0 \frac{\partial^2 s}{\partial t^2}, \tag{4}$$

and substituting Eq. (1c) into Eq. (4) yields the acoustic wave equation,

$$\nabla^2 p(\mathbf{r}, t) = \frac{1}{c_m^2} \frac{\partial^2 p(\mathbf{r}, t)}{\partial t^2}, \tag{5}$$

where c_m is the longitudinal wave velocity in the acoustic medium given by

$$c_m = \sqrt{\frac{\beta_0}{\rho_0} \gamma}, \tag{6}$$

as the adiabatic bulk modulus has the relation $B = \beta_0 \gamma$, with ρ_0 being the constant equilibrium density. Additionally, this is a characteristic property of the fluid and depends on the equilibrium conditions. Eq. (5) is also known as the homogeneous acoustic wave equation for pressures. For a linear acoustic pressure wave in a unit cell $p(\mathbf{r}, t)$, considering the harmonic case with time frequency ω; that is, $p(\mathbf{r}, t) = p(\mathbf{r})e^{-i\omega t}$, we obtain the stationary wave equation,

$$\nabla^2 p(\mathbf{r}) + k^2 p(\mathbf{r}) = 0, \tag{7}$$

being

$$k^2 = \left(\frac{\omega}{c_m}\right)^2, \tag{8}$$

the magnitude of the wave vector that gives us the dispersion relation as a function of the frequency ω and the wave speed in the medium c_m (for more detailed of acoustic wave equation deduction is suggested see (Ginsberg 2018a)). The only property of the medium that appears in Eq. (8) is the wave speed, which depends on conditions such as laboratory temperature and pressure and is closely related to the opposition that the medium presents to

the propagation of the pressure wave. That is why the specific acoustic impedance plays a fundamental role since it is the quotient between the acoustic pressure at a point in the medium and the instantaneous velocity of the particles at that point,

$$Z = \frac{p}{u}. \tag{9}$$

There are three limit cases for the acoustic impedance of a surface (Ginsberg 2018b); when the opposition of the medium is enormous, that is, it is not possible to disturb the medium for any pressure, it is said that the impedance $Z \to \infty$ and the surface is rigid; the opposite case of the soft surface occurs when $Z \to 0$, so a small pressure on surface induces a great speed. The third case is when the quotient of impedance is one, which represents a non-reflective medium. In addition, when impedance is finite and different from zero, a real material will be considered, and since we consider time-harmonic plane waves, the characteristic acoustic impedance is given by (Beranek and Mellow 2012)

$$Z_m = \rho c_m, \tag{10}$$

where the density ρ is the main constitutive parameter that determines the characteristics of the propagation of acoustic waves in the medium. The dispersion relation for real acoustic media for real constitutive media is obtained by substituting Eq. (10) into Eq. (8), given by

$$k = \frac{\rho_r}{Z_r} \frac{\omega}{c_m}, \tag{11}$$

where ρ_r and Z_r are the relative density and relative characteristic acoustic impedance of the medium in relation to air, respectively. Finally, when it comes to a system of this type, it is necessary to consider the boundary conditions at the interfaces between the media involved (Filippi et al. 1998),

$$p^{(1)} = p^{(2)}, \tag{12a}$$

$$\frac{c_{m_1}}{Z_{m_1}} \frac{\partial p^{(1)}}{\partial n} = \frac{c_{m_2}}{Z_{m_2}} \frac{\partial p^{(2)}}{\partial n}. \tag{12b}$$

The first condition tells us that the pressure is continuous on the interface, that is, there is no net force on the interface separating the media. The second condition tells us that the normal component of the pressure is continuous and requires that the media involved remain in contact (Kinsler et al. 2000).

In extreme cases of infinite or zero impedance (soft or rigid surface) the problem is significantly simplified. When there is a rigid surface, the normal pressure of the particles at the boundary

is zero; that is, the second boundary condition at the interface equals zero. Whereas, when there is a soft surface, the transmitted wave has zero pressure amplitude at the boundary, so the first condition at the interface equals zero (Pike and Sabatier 2001).

Let us also note the similarity between transverse electrical polarization (TE) with a surface considered as limits a perfect electric conductor is equivalent to the case of the soft acoustic surface; that is, a Dirichlet problem. In the same way, the transverse magnetic polarization (TM) is equivalent to the case of the rigid acoustic surface; that is, a Neumann problem (McGurn 2020).

NUMERICAL INTEGRAL METHOD

To calculate the corresponding pressure intensities of the eigenmodes of the system, we use the numerical technique of the IEM for a PnCW (Pérez-Aguilar *et al.* 2013). This technique is used, in particular, to model the interaction of waves that disturb a system with two-dimensional bodies (Pérez *et al.* 2009; Mendoza-Suárez and Pérez-Aguilar 2016). This method has two analogous approaches depending on whether the system is infinite or a finite length. The method is based on Green's second integral theorem in the equation that models our problem, allowing us to obtain a system of coupled integral equations. Subsequently, the discretization of the system of integral equations is carried out, which results in a set of linear equations under boundary conditions that can be represented in a single homogeneous matrix equation $MX = 0$ in the case of the infinite system, and inhomogeneous $MX = A$ for the finite system. It is important to mention that only a finite number of sampling points are taken into account along the contours that define the surface of the two-dimensional system of study, which allows savings in computational resources when numerically calculating line integrals in a discrete approximation form unlike differential methods that require a two-dimensional discrete mesh. Next, we describe the IEM corresponding to a two-dimensional PnCW of infinite and finite length.

Infinite waveguide

In Figure 1, P is the period of the PnCW system in x-direction; b is the distance between the flat plates; r is the radius of the circular inclusion, and the region enclosed by the curves Γ_i for $i = 1, 2, 3$ and 4 can be considered as an unit cell of the system. This region contains the circular inclusion with a profile given by Γ_5. Taking into account that the system is periodic along the direction of the waveguide, it is possible to apply Bloch's theorem (Bloch 1929), which states that the field can be written as a product of a plane wave and a periodic function along its direction of periodicity as

$$p(x + P, y) = p(x, y) \exp(-i\mathbf{K}P), \quad (13)$$

where $\mathbf{K}$ is the one-dimensional Bloch vector. For each j-th medium, the two-dimensional Green's function corresponds, which is the equivalent solution to Eq. (7), so the general form of the Helmholtz integral equation is

$$\frac{1}{4\pi} \oint_\Gamma \left[G\left(\mathbf{r}, \mathbf{r}'\right) \frac{\partial p\left(\mathbf{r}'\right)}{\partial n'} - p\left(\mathbf{r}'\right) \frac{\partial G\left(\mathbf{r}, \mathbf{r}'\right)}{\partial n'} \right] ds' = p(\mathbf{r})\Theta(\mathbf{r}), \quad (14)$$

with

$$G(R) = \frac{i}{4} H_0^1(kR), \quad (15)$$

where $H_0^1(\zeta)$ is the Hankel function of the first kind and zero order, $R = |\mathbf{r} - \mathbf{r}'|$ and $\Theta(\mathbf{r}) = 1$ if $\mathbf{r}$ is inside the region and $\Theta(\mathbf{r}) = 0$ otherwise. Given the geometry, the problem must be posed as a system of n equations (one for each region between

the interfaces of the different homogeneous media) in which the boundary conditions (Eqs. (12)) must be satisfied.

To solve the Eq. (14) numerically, it is necessary to discretize by dividing curve Γ of the j-th region into curve segments Γ_i of arc length Δs small enough so that the field and its normal derivative are constant. Thus, the integrals of Eq. (14) for the j-th region can be approximated as follows (Mendoza-Suárez *et al.* 2011)

$$\oint_\Gamma \left[G\left(\mathbf{r}, \mathbf{r}'\right) \frac{\partial E\left(\mathbf{r}'\right)}{\partial n'} \right] ds' \approx \sum_n \Phi_n L_{mn}, \quad (16a)$$

$$\oint_\Gamma \left[p\left(\mathbf{r}, \mathbf{r}'\right) \frac{\partial G\left(\mathbf{r}'\right)}{\partial n'} \right] ds' \approx \sum_n \Psi_{n'} N_{mn}, \quad (16b)$$

where the source functions are

$$\Phi_n = \left. \frac{\partial p\left(\mathbf{r}'\right)}{\partial n'} \right|_{\mathbf{r}' = \mathbf{r}'_n}, \quad (17a)$$

$$\Psi_n = \left. p\left(\mathbf{r}'\right) \right|_{\mathbf{r}' = \mathbf{r}'_n}, \quad (17b)$$

and matrix elements are defined as

$$L_{mn} = \int_{s_n - \Delta s/2}^{s_n + \Delta s/2} G\left(\mathbf{r}, \mathbf{r}'\right) ds', \quad (18a)$$

$$N_{mn} = \int_{s_n - \frac{\Delta s}{2}}^{s_n + \frac{\Delta s}{2}} \frac{\partial G\left(\mathbf{r}, \mathbf{r}'\right)}{\partial n'} ds'. \quad (18b)$$

In the previous expressions, the subscript m denotes the observation point and n the integration point. Substituting Eq. (15) in Eqs. (18) to obtain explicit forms, it is also necessary to consider that the Green function has a removable singularity in the two-dimensional case at $\mathbf{r} = \mathbf{r}'$; since this is where the point source that gives rise to this function is located. We then got the fact that Eqs. (18) are respectively (Mendoza-Suárez and Villa-Villa 2006)

$$L_{mn} = [1 - \delta_{mn}] \frac{i\Delta s}{4} H_0^{(1)} \left(k_j \left| \mathbf{r}_m - \mathbf{r}_n \right| \right) + \\ + \left[\frac{i\Delta s}{4} H_0^{(1)} \left(k_j \frac{\Delta s}{2e} \right) \right] \delta_{mn} \quad (19)$$

and

$$N_{mn} = [1 - \delta_{mn}] \frac{i\Delta s k_j}{4} \mathbf{n}_n \cdot \frac{(\mathbf{r}_m - \mathbf{r}_n)}{|\mathbf{r}_m - \mathbf{r}_n|_1} H_1^{(1)} \left(k_j \left| \mathbf{r}_m - \mathbf{r}_n \right| \right) + \\ + \left[\frac{1}{2} + \frac{\Delta s}{4\pi} \mathbf{n}_n \cdot \mathbf{t}'_n \right] \delta_{mn}, \quad (20)$$

where $\mathbf{n}_n$ is the normal to the contour Γ at the point $\mathbf{r}_n$ and $\mathbf{t}'_n$ is the curvature vector of the surface at the same integration point.

Therefore, we have converted the set of integral equations given by Eq. (14) into a homogeneous system of linear equations,

$$\sum_n \Phi_n L_{mn} - \sum_n p_n N_{mn} \approx p(\mathbf{r})\Theta(\mathbf{r}), \quad (21)$$

which can be represented by matrices such as

$$M\left(\mathbf{K}, \omega\right) X\left(\mathbf{K}, \omega\right) = 0, \quad (22)$$

where $M\left(\mathbf{K}, \omega\right)$ is the representative matrix associated with the system, $X\left(\mathbf{K}, \omega\right)$ are the source functions to be found that depend on the Bloch vector $\mathbf{K}$ and the frequency ω. Since the system of linear equations is homogeneous, a non-trivial solution can be obtained if the determinant of this matrix is zero. It is possible to determine the band structure, defining the function

$$D\left(\mathbf{K}, \omega\right) = \ln\left(\det M\left(\mathbf{K}, \omega\right)\right), \quad (23)$$

which presents local minimum points that will give the numerical dispersion relation $\omega(\mathbf{K})$, that determine the eigenmodes of the system for a specific frequency.

For the idealized cases where soft or rigid acoustic surfaces are present, which are characterized by having zero and infinite impedance respectively, the problem is significantly simplified. For example, in the case of the soft surface, the field is zero so there is no pressure inside the surface, on the other hand, in the case of the rigid surface, the normal derivative of the field is zero, so modes propagate even with the surface (Pike and Sabatier 2001).

Finite waveguide

Because in nature the dimensions of this type of system is finite, we can model a more realistic system taking the case of PnCW characterized by the number of consecutive unit cells to choose, thus we can truncate the infinite system to obtain a finite model of the waveguide as shown in Figure 2. Furthermore, we consider a plane pressure wave of pressure that interacts with the system at normal incidence; so in addition to the theory already mentioned, together with the fact that we are now dealing with matrix inversion problem (that is, a homogeneous matrix system) an incident pressure beam is considered (in region R_0) and calculation of scattered pressure field as response of the waveguide.

Since we have already described the integral numerical method, we use Eq. (14) in such a way that we can express the field in region R_0 as

$$p^{(0)}(\mathbf{r}) = p^{(0)}_{inc}(\mathbf{r}) + \frac{1}{4\pi} \sum_{j=1}^{M} \int_{\mathbf{r}_i} \left[G(\mathbf{r}, \mathbf{r}') \frac{\partial p(\mathbf{r}')}{\partial n'} - p(\mathbf{r}') \frac{\partial G(\mathbf{r}, \mathbf{r}')}{\partial n'} \right] ds'. \tag{24}$$

The terms on the right side correspond to the incident pressure field and the scattered pressure field, respectively. Then, for the other regions, when approximating to the observation point, we obtain

$$p^{(j)}(\mathbf{r})\Theta_j(\mathbf{r}) = \frac{1}{4\pi} \oint_{\mathbf{r}_i} \left[\frac{\rho_{r,j}}{Z_{r,j}} G_j(\mathbf{r}, \mathbf{r}') \frac{\partial p_j(\mathbf{r}')}{\partial n'} - p_j(\mathbf{r}') \frac{\partial G_j(\mathbf{r}, \mathbf{r}')}{\partial n'} \right] \delta_{ji} ds', \tag{25}$$

where $\Theta_j(\mathbf{r}) = 1$ if $\mathbf{r}$ is inside the j-th medium or zero otherwise, δ_{ji} is the Kronecker delta and $\rho_{r,j}$, $Z_{r,j}$ are the density and impedance of the j-th medium relative to that of air, respectively. With this the inhomogeneous algebraic system is found that has the field and its normal derivative as unknowns.

To deal with the finite PnCW problem with method described above, it is necessary to make assumptions about the incident pressure field. Once the sources $\Psi_n^{(j)}$ and $\Phi_n^{(j)}$ are obtained, with $j = 1, 2, \ldots, M$ bodies (using the notation of Eqs. (17)), the field can be calculated at any point within the pressure regions that constitute the system using the same integral equations. If $\mathbf{r} \in R_0$, that is, the propagation region, the corresponding equation is

$$\Psi_m^{(0)} = \sum_{n=1}^{N} L_{mn}^{(0)} \Phi_n^{(0)} - \sum_{n=1}^{N} N_{mn}^{(0)} \Psi_n^{(0)} - \Psi_m^{\text{inc}(0)}, \tag{26}$$

where, the incident pressure field is expressed as

$$\Psi^{(\text{inc})}(\mathbf{r}) = \Psi_0 e^{i\mathbf{k}\cdot\mathbf{r}}, \tag{27}$$

where Ψ_0 is a constant with appropriate units, $\mathbf{k}$ is the propagation wave vector and $\mathbf{r}$ is the position of each point at which the wave comes into contact. On the other hand, for the other regions $\mathbf{r} \in \mathbf{R}_j$, the associated equation is

$$\Psi_m^{(j)} = \sum_{n=1}^{N} L_{mn}^{(j)} \Phi_n^{(j)} - \sum_{n=1}^{N} N_{mn}^{(j)} \Psi_n^{(j)}. \tag{28}$$

RESULTS

In the programming of the integral equation method, the Message Passing Interface (MPI) protocol was implemented to reduce the computation time for obtaining results. To obtain reliable results in the case of high frequencies, it is necessary to use small discretization intervals Δs. To ensure the accurate approximation of the integral corresponding to the profile that models the system, the intervals must be smaller than the periodicity of the system, which is related to the wavelength $\lambda = 2\pi c_m / \omega$. Thus, it is necessary that $\Delta s \ll \lambda$. Furthermore, since statistical properties envision disordered behavior in systems where chaos phenomenon occurs, we calculated the average of the ACF for several data sets. This tells us the similarity between the behavior of the function at a given point and its behavior at any consecutive point.

Autocorrelation Function

An important mathematical tool for the interpretation of numerical data is the ACF. The ACF defines how data points in a spatial (or temporal) series relate, on average, to previous data points. In other words, it measures the self-similarity of the data set (Vilela et al. 2013).

The ACF for a pattern of acoustic pressure field intensity, $I(\mathbf{r})$, in the unit cell is defined as:

$$ACF_j \equiv \sum_{i=1}^{N_p} \frac{\left(I(\mathbf{r}_i) - \mu \left(I(\mathbf{r}_{i-j}) - \mu \right) / N_p \right)}{\sigma^2}, \tag{29}$$

being the average value of I,

$$\mu = \sum_{i=1}^{N_p} \frac{I(\mathbf{r}_i)}{N_p} \tag{30}$$

and the variance,

$$\sigma^2 = \sum_{i=1}^{N_p} \frac{\left(I(\mathbf{r}_i) - \mu \right)^2}{N_p}, \tag{31}$$

where Np is the number of sampling points with coordinates $(x_i, y(x_i))$. In this case $y(x)$ being fixed, with $0 < x < P$ in the infinite system and $0 < x < 10P$ in the finite system and the subscript j indicates the value of the ACF with respect to the j-th coordinate point. In this way, autocorrelation was calculated using points located in the upper middle section of the waveguide. The autocorrelations of the intensity patterns that we will show in this work result from correlations between the values of intensity $I(\mathbf{r})$ themselves. The ACF is positive when the relationship between values is linear (they are very similar), it is negative when the relationship is linearly inverse (they are very different) and it is null when there is no linear relationship (Montenegro-García 1989; Legendre 1993). A quantity that could be even more important is the standard deviation of the ACF, known as *correlation length* l_c, which helps us to compare the cases considered since it is a measure used to quantify the dispersion of a set of numerical data (Doya et al. 2002a). Due to the oscillatory nature of the ACF, the
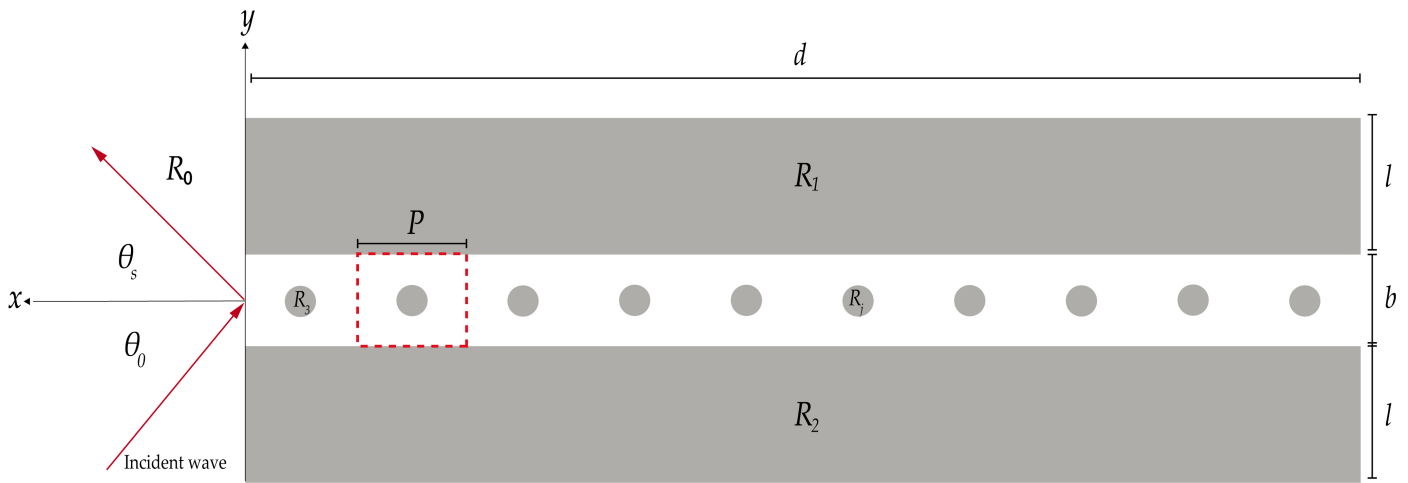
Figure 2 Finite 2D PnCW system diagram.

length of the correlation is related to the typical speckle grain size. Therefore, the decrease in the length of the correlation as the frequency increases is a characteristic feature of chaos or equivalently of the presence of a positive Lyapunov exponent (Sugihara and May 1990).

Infinite PnCW

Let us consider the system illustrated in Figure 1 with a periodicity $P = 2\pi \ \mu$m in one direction, a plate spacing $b = 2\pi \ \mu$m, a periodic arrangement of circular inclusions with a filling fraction f for a sufficiently small discretization step $\Delta s = 0.0126 \ \mu$m for better data acquisition. Furthermore, the determinant function $D \ (k_r = 0, \omega_r)$ was calculated for a number of frequencies given by $n_\omega = 400$ choosing a particular propagation mode given by $(k_r = 0, \omega_r)$. The system is modeled in particular for a brass inclusion, however, it is possible to apply the method for different types of materials considering the characteristic acoustic impedance of the inclusion. In the case of brass it is given by a value of $Z = 40$ MRayls, which is a real rigid surface; while the top and bottom plates of the system are composed of an ideal soft acoustic material.

First, the inclusion centered on the unit cell with a filling fraction factor of $f = 0.003$ is considered. The pressure field intensities as well as the ACFs are obtained. The numerical results obtained range for frequencies from 504.8964 MHz to $\omega = 199.308$ GHz (from ultrasound to hypersonic) are shown in Figure 3. Data sets are taken along 1200 different lines parallel to x that are equidistant a distance $\varepsilon > 0$. Each of the ACFs are calculated from $N_P = 3063$ sampling points and the ACFs are averaged showing behavior that tends to zero with increasing frequency. Similarly, pressure field intensity patterns are obtained for a brass inclusion with a larger value of the filling fraction factor $f = 0.3$, leading to different vibration modes as seen in Figure 4. The parameters used and obtained are compiled in Table 1 for both cases.

The numerical results of infinite PnCW with different filling fractions shown in both tables indicate that the value of the correlation length is smaller as the frequency increases. Such decrease in the correlation length deduced from the standard deviation of the spatial ACF with increasing frequency is a characteristic feature of chaos (or equivalently, of the presence of a positive Lyapunov exponent) (Sugihara and May 1990). Furthermore, it complies with the

acoustic-classical correspondence of the already known properties of the eigenvalues and eigenfunctions of the Sinai billiard-shaped cavities. This also provides further evidence that the acoustic modes in a PnCW at high frequencies (small wavelengths) is a deterministically chaotic system.

To break the symmetry of the unit cell, the inclusion is placed in the upper right corner of the unit cell for both values of the filling fractions previously considered. Observing in Figures 5 and 6 how field pressure patterns change as the frequency ω increases, we see that modes inside the inclusion in some cases differ greatly from the form held outside it. However, the continuity of the field is maintained by boundary conditions. Table 2 shows the values obtained for both figures.

■ Table 1 Numerical results of infinite PnCW with centered brass inclusion.

f	ω (MHz)	l_c
0.003	504.8964	0.37695
0.003	16958.3923	0.12054
0.003	66640.7837	0.06492
0.003	199308.6716	0.0555
0.3	509.2547	0.38954
0.3	16957.3781	0.11355
0.3	66640.9522	0.16325
0.3	199229.8121	0.10516

Finite PnCW

Let us now consider a more realistic system, such as the finite PnCW of length $d = 20\pi \ \mu$m, plate spacing $b = 2\pi \ \mu$m, which
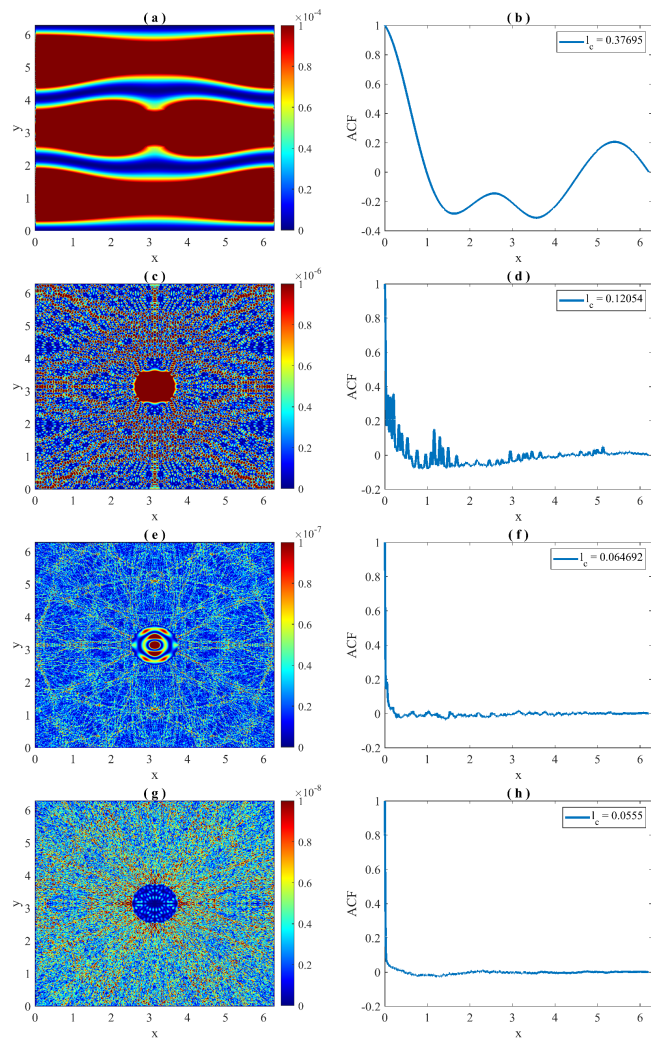
Figure 3 Pressure field intensity patterns and their respective ACFs for an infinite PnCW with small brass inclusion ($f = 0.003$) centered on the unit cell. The frequency values chosen for each field pattern are indicated in Table 1.

■ **Table 2 Numerical results of infinite PnCW with non-centered brass inclusion.**

f	ω (MHz)	l_c
0.003	491.8217	0.38589
0.003	16956.8086	0.087289
0.003	66629.7729	0.071931
0.003	199323.604	0.050629
0.3	601.8675	0.31883
0.3	16953.4455	0.132
0.3	66646.2891	0.12757
0.3	199323.604	0.069709
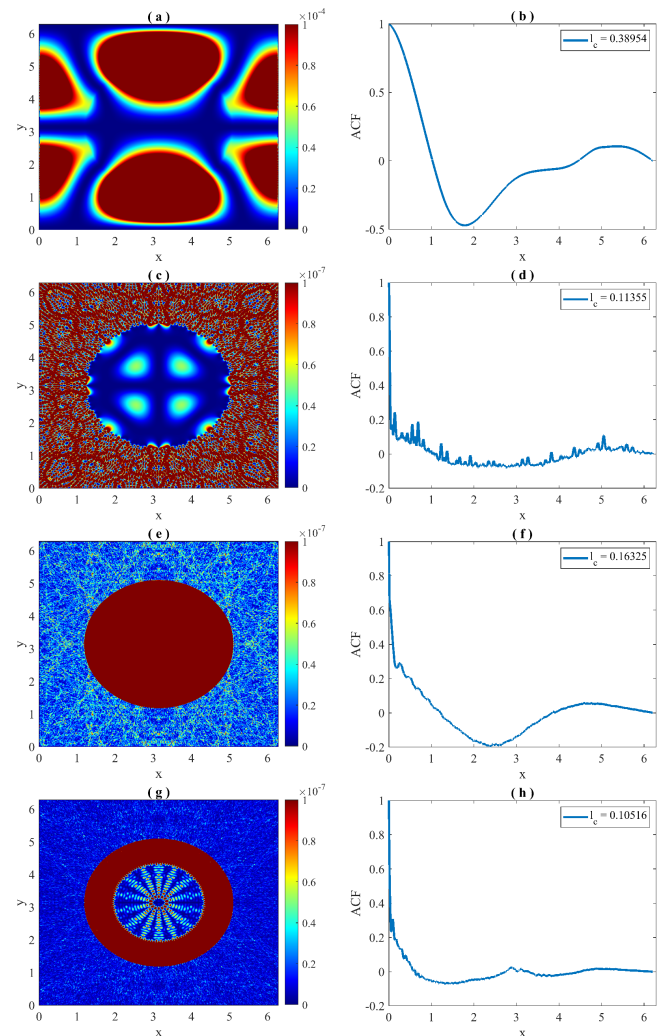
Figure 4 Pressure field intensity patterns and their respective ACFs for an infinite PnCW with a large brass inclusion ($f = 0.3$) centered on the unit cell. The frequency values chosen for each field pattern are indicated in Table 1.
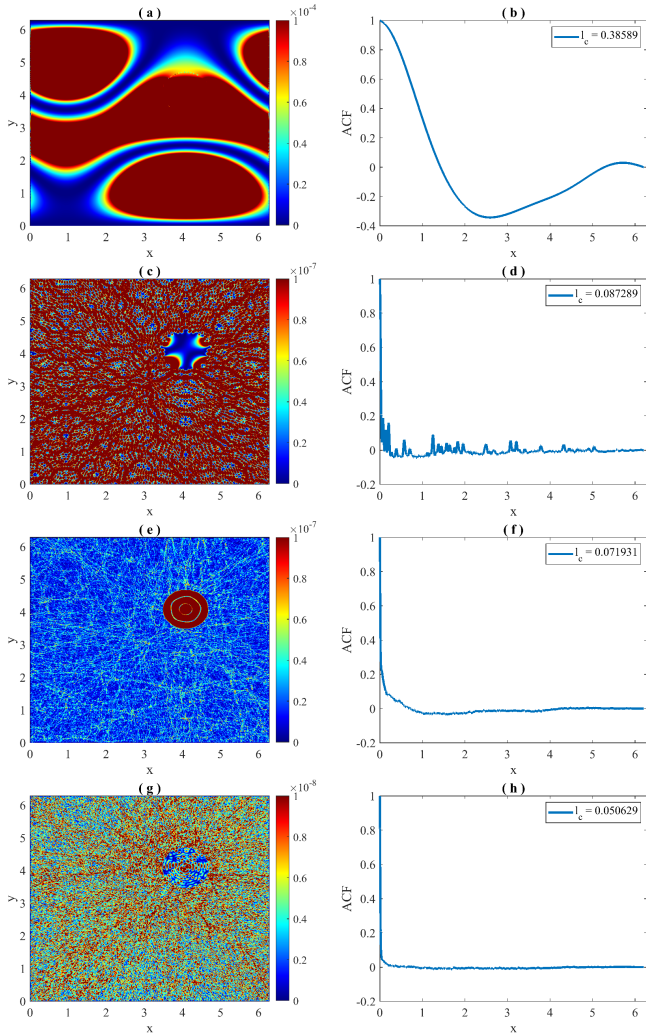
Figure 5 Pressure field intensity patterns and their respective ACFs for an infinite PnCW with small brass inclusion ($f = 0.003$) non centered on the unit cell. The frequency values chosen for each field pattern are indicated in Table 2.

Figure 6 Pressure field intensity patterns and their respective ACFs for infinite PnCW with a large brass inclusion ($f = 0.3$) non centered on the unit cell. The frequency values chosen for each field pattern are indicated in Table 2.

have a thickness of $l = 30$ μm to avoid edge effects and 10 brass inclusions with filling fraction of $f = 0.3$ distributed by a period $P = 2\pi$ and the discretization of the mesh given by $\Delta s = 0.00338$ μm (see Figure 2).

As in the finite system, brass inclusions are considered, while the plates are made of soft acoustic material. The pressure field intensities that were obtained for frequencies from $\omega = 830$ MHz to 66 GHz are shown in Figure 7. The values considered for the case of a finite PnCW are shown in Table 3. The respective ACFs are calculated from $N_P = 6254$ sampling points in the same way over the average of 1200 ACFs of the data set within the PnCW. From the average of the ACFs, the minimum correlation length of $l_c = 0.034718$ corresponding to the highest frequency is obtained. Similar to the case of the infinite system, in both cases the increase in frequency results in a decrease in the correlation length, which we also attribute to the fact that the system response is chaotic.

■ **Table 3 Numerical results of finite PnCW with centered brass inclusion.**

f	ω (MHz)	l_c
0.3	830.269	0.20757
0.3	8459.2819	0.087232
0.3	16742.771	0.065393
0.3	33153.8227	0.038081
0.3	66260.371	0.034718
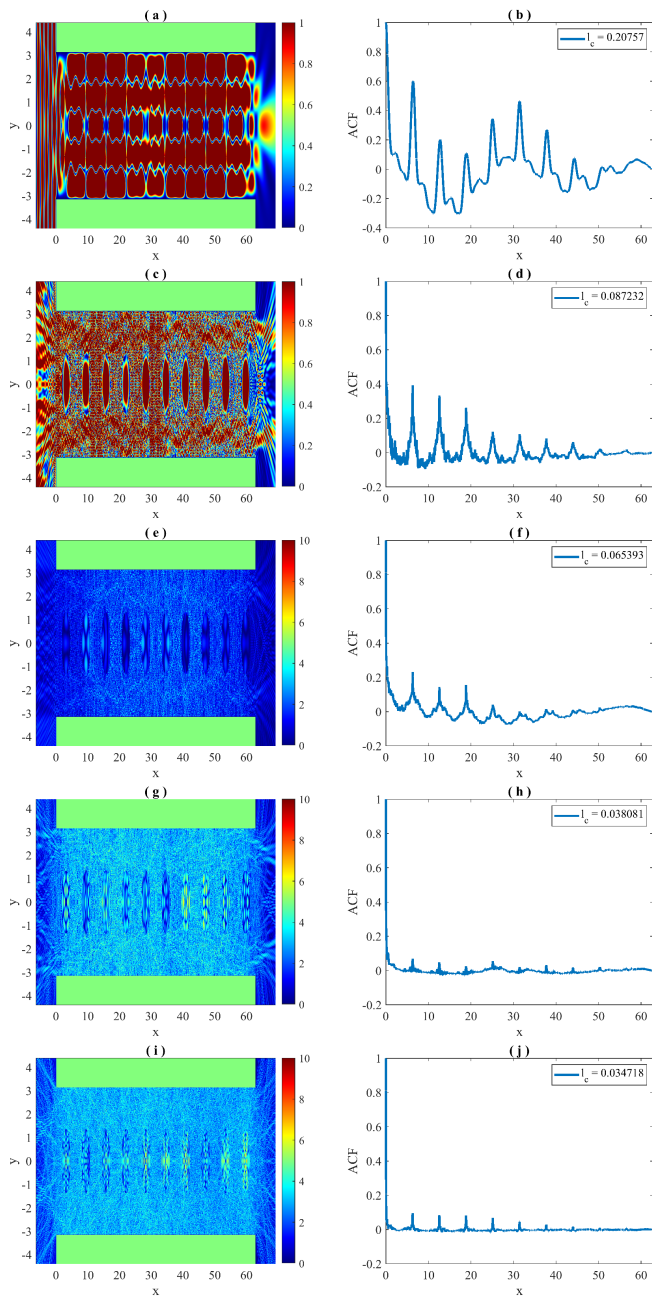
Figure 7 Pressure field intensity patterns and their respective ACFs for a finite PnCW with 10 large brass inclusion ($f = 0.3$) centered on the waveguide. The frequency values chosen for each field pattern are indicated in Table 3.

CONCLUSION

We conducted a theoretical and numerical study to analyze the chaotic effects in phononic crystal waveguides composed of two plane-parallel plates and a periodic arrangement of circular cylindrical inclusions with acoustic surfaces of real materials. We used the numerical integral method to study the acoustic response of the system and examine the chaos phenomenon present in it. In our simulations, we have observed that the periodic arrangement of circular cylindrical inclusions in our acoustic systems has a notable impact on the pressure field intensity patterns as the frequency increases. This effect has been studied using the ACF and

it has been observed that the correlation length decays at higher frequencies in both types of systems considered. This behavior is an indication of the presence of chaotic behavior in the system due to non-periodicity and disordered response. These findings support our initial hypothesis and demonstrate that inclusions in the system introduce complex and chaotic dynamics in the propagation of acoustic waves. Our study has also revealed that the size and arrangement of circular cylindrical brass inclusions influence the acoustic response of the system. By changing the radius and position of the inclusions, significant changes in the intensity of the acoustic pressure field can be obtained. In summary, numerical analysis using the Integral Equation Method has allowed us to better understand the behavior of two-dimensional PnCW acoustic systems. This approach offers opportunities for design and optimization of acoustic devices with customized properties, and their application in fields such as sound engineering, acoustic communication, and noise control. Furthermore, the phenomenon of chaotic dynamics in PnCW could give rise to applications such as the detection of defects in crystal geometry with ACF, the transmission and control of acoustic waves with metamaterials (Deymier 2013), or information encryption (Bose and Pathak 2006; Zhou *et al.* 2014).

Availability of data and material

Not applicable.

Conflicts of interest

The authors declare that there is no conflict of interest regarding the publication of this paper.

Ethical standard

The authors have no relevant financial or non-financial interests to disclose.

LITERATURE CITED

Beranek, L. L. and T. Mellow, 2012 *Acoustics: sound fields and transducers*. Academic Press.

Berry, M. V., 1977 Regular and irregular semiclassical wavefunctions. Journal of Physics A: Mathematical and General **10**: 2083–2091.

Blackstock, D. T., 2001 Chapter 2 Detailed Development of Acoustical Wave Equations, pp. 65–107 in *Fundamentals of Physical Acoustics*, Acoustical Society of America.

Bloch, F., 1929 Über die quantenmechanik der elektronen in kristallgittern. Zeitschrift für physik **52**: 555–600.

Bose, R. and S. Pathak, 2006 A novel compression and encryption scheme using variable model arithmetic coding and coupled chaotic system. IEEE Transactions on Circuits and Systems I: Regular Papers **53**: 848–857.

Chen, M., H. Jiang, H. Zhang, D. Li, and Y. Wang, 2018 Design of an acoustic superlens using single-phase metamaterials with a star-shaped lattice structure. Scientific reports **8**: 1–8.

de Rosny, J., A. Tourin, and M. Fink, 2000 Coherent backscattering of an elastic wave in a chaotic cavity. Physical review letters **84**: 1693–1695.

Dembowski, C., H.-D. Gräf, A. Heine, R. Hofferbert, H. Rehfeld, *et al.*, 2000 First experimental evidence for chaos-assisted tunneling in a microwave annular billiard. Physical review letters **84**: 867.

Deymier, P. A., 2013 *Acoustic metamaterials and phononic crystals*, volume 173. Springer Science & Business Media.

Doya, V., O. Legrand, and F. Mortessagne, 2002a Light scarring in an optical fiber. Physical Review Letters **88**: 014102.

Doya, V., O. Legrand, F. Mortessagne, and C. Miniatura, 2002b Speckle statistics in a chaotic multimode fiber. Physical Review E **65**: 056223.

El-Kady, I., R. Olsson III, and J. Fleming, 2008 Phononic band-gap crystals for radio frequency communications. Applied Physics Letters **92**: 233504.

Ellegaard, C., K. Schaadt, and P. Bertelsen, 2001 Acoustic chaos. Physica Scripta **2001**: 223–230.

Filippi, P., A. Bergassoli, D. Habault, and J. P. Lefebvre, 1998 *Acoustics: basic physics, theory, and methods*. Elsevier.

Ginsberg, J. H., 2018a Chapter 4 Principles and Equations for Multidimensional Phenomena, pp. 295–346 in *Acoustics: A Textbook for Engineers and Physicists*, Springer.

Ginsberg, J. H., 2018b *Acoustics: A Textbook for Engineers and Physicists*, volume 1. Springer.

He, J., S. Yang, Z. Hileman, R. Wang, D. Homa, *et al.*, 2020 An acoustic waveguide with tight field confinement for high temperature sensing. IEEE Sensors Journal **20**: 14126–14131.

Heller, E. J., 1984 Bound-state eigenfunctions of classically chaotic hamiltonian systems: scars of periodic orbits. Physical Review Letters **53**: 1515–1518.

Hensinger, W. K., H. Häffner, A. Browaeys, N. R. Heckenberg, K. Helmerson, *et al.*, 2001 Dynamical tunnelling of ultracold atoms. Nature **412**: 52–55.

Jia, Z., Y. Chen, H. Yang, and L. Wang, 2018 Designing phononic crystals with wide and robust band gaps. Physical Review Applied **9**: 044021.

Jing, L., Z. Li, Y. Li, and R. D. Murch, 2018 Channel characterization of acoustic waveguides consisting of straight gas and water pipelines. IEEE Access **6**: 6807–6819.

Kaplan, L., 1998 Wave function intensity statistics from unstable periodic orbits. Physical review letters **80**: 2582–2585.

Kaplan, L. and E. Heller, 1999 Measuring scars of periodic orbits. Physical Review E **59**: 6609–6628.

Khelif, A., A. Choujaa, S. Benchabane, B. Djafari-Rouhani, and V. Laude, 2004 Guiding and bending of acoustic waves in highly confined phononic crystal waveguides. Applied physics letters **84**: 4400–4402.

Kinsler, L. E., A. R. Frey, A. B. Coppens, and J. V. Sanders, 2000 *Fundamentals of acoustics*. John Wiley & Sons.

Kittel, C., P. McEuen, and P. McEuen, 1996 *Introduction to solid state physics*, volume 8. Wiley New York.

Kudrolli, A., M. C. Abraham, and J. P. Gollub, 2001 Scarred patterns in surface waves. Physical Review E **63**: 026208.

Kuhl, U., H. Stöckmann, and R. Weaver, 2005 Classical wave experiments on chaotic scattering. Journal of Physics A: Mathematical and General **38**: 10433.

Lee, H. S., D. H. Luong, M. S. Kim, Y. Jin, H. Kim, *et al.*, 2016 Reconfigurable exciton-plasmon interconversion for nanophotonic circuits. Nature communications **7**: 13663.

Legendre, P., 1993 Spatial autocorrelation: trouble or new paradigm? Ecology **74**: 1659–1673.

Liu, J., H. Guo, and T. Wang, 2020 A review of acoustic metamaterials and phononic crystals. Crystals **10**: 305.

Maldovan, M., 2013 Sound and heat revolutions in phononics. Nature **503**: 209–217.

McGurn, A. R., 2020 *Introduction to Photonic and Phononic Crystals and Metamaterials*. Morgan & Claypool Publishers.

Mendoza-Suárez, A. and H. Pérez-Aguilar, 2016 Numerical integral methods to study plasmonic modes in a photonic crystal waveguide with circular inclusions that involve a metamaterial. Photonics and Nanostructures-Fundamentals and Applications **21**: 1–12.

Mendoza-Suárez, A., H. Pérez-Aguilar, and F. Villa-Villa, 2011 Optical response of a perfect conductor waveguide that behaves as a photonic crystal. Progress In Electromagnetics Research **121**: 433–452.

Mendoza-Suárez, A. and F. Villa-Villa, 2006 Numerical method based on the solution of integral equations for the calculation of the band structure and reflectance of one- and two-dimensional photonic crystals. Journal of the Optical Society of America B **23**: 2249–2256.

Montenegro-García, A., 1989 La función de autocorrelación y su empleo en el análisis de series de tiempo. Revista Desarrollo y Sociedad pp. 117–132.

Mukhin, N., M. Kutia, A. Aman, U. Steinmann, and R. Lucklum, 2022 Two-dimensional phononic crystal based sensor for characterization of mixtures and heterogeneous liquids. Sensors **22**: 2816.

Navarro-Urrios, D., N. E. Capuj, M. F. Colombano, P. D. García, M. Sledzinska, *et al.*, 2017 Nonlinear dynamics and chaos in an optomechanical beam. Nature communications **8**: 14965.

Nöckel, J. U. and A. D. Stone, 1997 Ray and wave chaos in asymmetric resonant optical cavities. Nature **385**: 45–47.

Otsuka, P. H., K. Nanri, O. Matsuda, M. Tomoda, D. Profunser, *et al.*, 2013 Broadband evolution of phononic-crystal-waveguide eigenstates in real-and k-spaces. Scientific reports **3**: 3351.

Pennec, Y., B. D. Rouhani, E. El Boudouti, C. Li, Y. El Hassouani, *et al.*, 2010a Simultaneous existence of phononic and photonic band gaps in periodic crystal slabs. Optics express **18**: 14301–14310.

Pennec, Y., J. O. Vasseur, B. Djafari-Rouhani, L. Dobrzyński, and P. A. Deymier, 2010b Two-dimensional phononic crystals: Examples and applications. Surface Science Reports **65**: 229–291.

Pérez, H. I., C. I. Valencia, E. R. Méndez, and J. A. Sánchez-Gil, 2009 On the transmission of diffuse light through thick slits. Journal of the Optical Society of America A **26**: 909–918.

Pérez-Aguilar, H., A. Mendoza-Suárez, E. S. Tututi, and I. F. Herrera-González, 2013 Disordered field patterns in a waveguide with periodic surfaces. Progress In Electromagnetics Research B **48**: 329–346.

Pike, E. R. and P. C. Sabatier, 2001 *Scattering, Two-Volume Set: Scattering and Inverse Scattering in Pure and Applied Science*. Elsevier.

Ruelle, D., 1991 *Chance and Chaos*, volume 110. Princeton University Press.

Sinai, Y. G., 1970 Dynamical systems with elastic reflections. Russian Mathematical Surveys **25**: 137–189.

Sridhar, S., 1991 Experimental observation of scarred eigenfunctions of chaotic microwave cavities. Physical review letters **67**: 785–788.

Sridhar, S. and W. Lu, 2002 Sinai billiards, ruelle zeta-functions and ruelle resonances: microwave experiments. Journal of statistical physics **108**: 755–765.

Stöckmann, H.-J., 1999 *Quantum Chaos: An Introduction*. Cambridge University Press, New York.

Sugihara, G. and R. M. May, 1990 Nonlinear forecasting as a way of distinguishing chaos from measurement error in time series. Nature **344**: 734.

Torrent, D. and J. Sánchez-Dehesa, 2008 Acoustic cloaking in two dimensions: a feasible approach. New Journal of Physics **10**: 063015.

Vilela, M., N. Halidi, S. Besson, H. Elliott, K. Hahn, *et al.*, 2013 Fluctuation analysis of activity biosensor images for the study of information flow in signaling pathways. In *Methods in enzymology*, volume 519, pp. 253–276, Elsevier.

Villa-Villa, F., H. Pérez-Aguilar, and A. Mendoza-Suárez, 2017 The locally corrected Nyström method applied to 3D scalar SIE in acoustic cavities using curvilinear coordinates. Engineering Analysis with Boundary Elements **79**: 110–118.

Weaver, R. L., 1989 Spectral statistics in elastodynamics. The Journal of the Acoustical Society of America **85**: 1005–1013.

Wilkinson, P., T. Fromhold, L. Eaves, F. Sheard, N. Miura, *et al.*, 1996 Observation of 'scarred' wavefunctions in a quantum well with chaotic electron dynamics. Nature **380**: 608–610.

Zaki, S. E., A. Mehaney, H. M. Hassanein, and A. H. Aly, 2020 Fano resonance based defected 1D phononic crystal for highly sensitive gas sensing applications. Scientific Reports **10**: 17979.

Zhou, Y., Z. Hua, C.-M. Pun, and C. P. Chen, 2014 Cascade chaotic system with applications. IEEE transactions on cybernetics **45**: 2001–2012.